2528-9705

Örgütsel Davranış Araştırmaları Dergisi
Journal Of Organizational Behavior Research
Cilt / Vol.: 3, Sayı / Is.: S2, Yıl/Year: 2018, Kod/ID: 81S2373

LOCATING SINGLE PHASE TO GROUND FAULT IN THREE-PHASE UNDERGROUND POWER CABLES USING MODAL THEORY AND FOURIER TRANSFORM

Ebadollah AMOUZAD MAHDIRAJI*, Sirus MOHAMMADI SHAH KILAH, Amine Sadat HOSSEINI

Department of Engineering, Sari Branch, Islamic Azad University, Sari, Iran.

*Corresponding Author
Email: Ebad.Amouzad@gmail.com

ABSTRACT

One of the most commonly used equipment in the power system, which is exposed to various types of faults for various reasons, is high and low voltage pressure cables. Due to the fact that cables, either power or distribution cables are mostly transported from underground, despite their further reliability in airway, they are more difficult to repair and possibly replace in case of fault, in line with this the correct fault detection and location of them is of utmost important. In this paper, as is clear from the title of the research, the Fourier transform and Modal transform methods are used to find the type and location of faults, so that the efficiency of the selected method for detecting and locating the faults in underground transmission cables is examined and the speed and accuracy of finding a solution to the problem is assessed. In this thesis, it is expected that the Fourier transform method, followed by the Modal transform has substantial speed and accuracy in determining the type and location of the faults. Meanwhile, the detection and location indicators are used to determine the type and location of the fault, which as shown in the simulations, will have efficient performance. The sample model is simulated to demonstrate the correctness of these methods. The simulation results from MATLAB and EMTP/ATP software confirm the precise and rapid performance of the proposed method.

Keywords: *Power Cables, Short Circuit Fault, Fourier Transform, Clarke Transform, Modal Components, Fault Detection and Localization Indicators*

INTRODUCTION

In ANSI/IEEE Std.100-1992 standard fault is defined as a physical condition that results in the failure of a device, a component, or an element to perform a necessary routine. A short or definitive wire termination includes this definition. A fault almost always involves a short circuit between electric phase conductors or between a phase and ground. The fault may be a screw connection or may have some impedance at the fault location. The term “fault” which is used as the “short circuit” synonym is defined in the abovementioned standards (Hassan Sayed Barakat, 2014). Due to the defects that occur in ground cables, the type of methods used to determine the location of defects will also be different. So, firstly, the kind of defect which has appeared in the cable should be determined (Kuan and Warwick, 1992). Generally, methods for determining the location of faults for cables, are divided into online and offline methods. In offline method, special tools are used to test the cable failure while in the online method; the voltage and current are sampled and processed to determine the fault point (Underground cable fault location reference manual, 1995). A location algorithm based on the two ends of

Geliş tarihi/Recieved: 10.12.2017 – Kabul tarihi/Accepted: 09.02.2018 – Yayın tarihi/Published: 21.08.2018

cable is presented especially for the life-long power cables. The aging process in cable causes a change in the relative passivity coefficient and consequently leads to a change in capacitance of the positive, negative and zero capacitors. The fault location design is based on the measurement of phasors from both ends of the cable in combination with the linear distribution model; Clarketransform and Discrete Fourier Transform Theory (DFT) (Aziz et al., 2006). In the reference (Yang et al., 2008) which differs from impedance-based methods, a repeatable algorithm is proposed for fault localization in cable. The circuit is modeled by distributed parameter method and the voltage and the current equations are formulated based on the sequential networks. The Newton-Raphson method is used to calculate the fault distance. The algorithm also extends to radial multi-section cables with light loads. Other works which have been implemented in exploiting the Allindar Dutch Network are presented in (Provoost and Van Buijtenen, 2009; Van Oirsouw and Provoost, 2003). Fault locators use only the calculated reactance. Since the fault impedance reactance is zero and the cable reactance is also specified and is not dependent on the current, short circuit scenarios are simulated in all nodes in a faulty feeder in a real network model. The calculated impedance is compared with the simulated impedance to find the exact location. This algorithm finds the distance location within 5 minutes after the occurrence of the fault. Another valid way of mobile waves is by changing the energy stored in the capacitor and inductor, which is produced on the lines or cables after the fault occurs. Both the voltage and the current waves propagate along the circuit at a velocity to that of a light, so as to encounter the impedance discontinuities, and then high frequency waves emanating from the fault are reflected and transferred to the other. Almost all the methods based on mobile waves follow the principle of Boolean diagram (Bewley, 1931) and the fault distance is obtained by the product of the propagation velocity and the time interval of the fault which is equal to the time difference between the instant of the initial arrival of the wave-front and the moment the wave-front is reflected. Principles of the basic locating and a variety of convention locating methods are introduced in (Gale et al., 1993).

In this paper, a 230 kV transmission network along with two sources at the two ends of the line (representing a power network on both sides) was first simulated in EMTP/ATP transient states software and then using the MATLAB software, time outputs of this software are transmitted via transmitting the Fourier transform to phasor domain. Finally, using the detection and fault localization indicators, the type and location of the faults are recognized. The simulation results are presented in different figures and tables for several fault samples and different times with different fault resistances.

Fourier Transform

In general, Discrete Fourier Transform (DFT) is defined as follows (Phadke and Thorp, 2008):

$$X(\omega)=\sum_{n=-\infty}^{\infty} x[n]e^{-i\omega n} \qquad (1)$$

The above relation is considered as the main definition of the Fourier transform which is expressed in terms of discrete signals. If a signal is in a continuous form of x(t), in order to obtain a discrete Fourier transform, first a discrete signal x′(kΔt) is considered which includes N sample of the sampled signal x(t), the amount of which is expresses over time in relation (2):

$$x'(k\Delta T)=x(t)w(t)\sum_{k=-\infty}^{+\infty}\delta(t-k\Delta T) \tag{2}$$

Where ΔT is the sampling period and w(t) is the function that contains N sample of the sampled signal of x(t) at the time interval T_0, that is, this function can be introduced as a function with the sampling window to N length. For stable applications, the length of the sampling window is constant but this window moves forward over time and the samples from -∞ to ∞ enter and exit from the window, respectively and thus the sampling process is accomplished within time domain. Fourier transform of the sampled signal is expressed in the following relation, as defined in (3):

$$X'(f)=\sum_{k=-\infty}^{+\infty}a_k\delta(f-\frac{k}{T_0})$$
$$a_k=\frac{1}{T_0}\int_{-T_0/2}^{T_0/2}\left[\sum_{k=0}^{N-1}x(t)\times\delta(t-k\Delta T)\right]e^{-\frac{j2k\pi t}{T_0}}dt \tag{3}$$

Having simplified the formula (3) and considering NΔT= T_0, the relation of discrete Fourier transform is expressed as (4). Therefore, the discrete Fourier transform of the signal $x'(k\Delta t)$ will be as follows (5). But the general form of calculating the discrete Fourier transform that most of the authors use is as relation (6).

$$a_n=\sum_{k=0}^{N-1}x(k\Delta T)e^{\frac{-j2nk\pi}{N}}\qquad n=0,\pm1,\pm2,... \tag{4}$$

$$X'(\frac{n}{T_0})=\sum_{k=0}^{N-1}x(k\Delta T)e^{\frac{-j2kn\pi}{N}}\qquad n=0,1,2,...N-1 \tag{5}$$

$$X(r)\Big|_{t=(r-1)\Delta T}=\frac{2}{N}\sum_{k=0}^{N-1}x(r+k)e^{-\frac{2\pi}{N}jk}\quad,\ r\geq1 \tag{6}$$

In the above relation, t=(r-1) ΔT is the phasor time tag of the r^{th} sample. ΔT is equal to $1/f_s$, the distance between each two sampled signal. N is the number of the samples in each sampling cycle which is specified considering the sampling frequency (f_s) and power frequency (f) $N=\frac{f_s}{f}$. In the above relation, x(r+k) is also $r+k^{th}$ samplefrom the sampled signal of x(n). For example, for the first phasor x (1) calculated at zero time, it can be written in relation (7). It should be noted that the above relation is suitable for offline applications because it uses changes in subsequent samples in the calculation of phasor and there is no delay in in following the signal changes. In real-time and immediate applications, the subsequent samples do not exist in waveform that can be used to calculate the phasor, but the discrete Fourier transform algorithm from the previous samples to the former cycle is used, so there is a delay of NΔT seconds, unless the sampling window changes in accordance with sample variation. To adapt

with the actual conditions, the phasors obtained with the labels can be delayed by NΔT seconds or the relation (8) can be used for real time use:

$$X(1)\big|_{t=0} = \frac{2}{N}\sum_{k=0}^{N-1} x(1+k)e^{-j\frac{2\pi}{N}k} = \frac{2}{N}[x(1)e^{-j0} + x(2)e^{-j\frac{2\pi}{N}} + \ldots + x(N)e^{-j\frac{2\pi}{N}(N-1)}] \quad (7)$$

$$X(r)\big|_{t=(r-1)\Delta T} = \frac{2}{N}\sum_{k=0}^{N-1} x\left[(r-1+k-N)\Delta T\right]e^{-\frac{2\pi}{N}jk} \quad , \; r \geq 1 \quad (8)$$

Clarke Transform

The three-phase lines have considerable electromagnetic coupling. In order to eliminate the coupling effect between phases and employ the mobile wave method, the signals of phase domain are converted into modal component by a Modal transform. It is one of the famous transformations that has been used in this paper. The independence of these quantities makes any mode of calculation easy and is not influenced by other modes. Having used this transformation, the fault calculation can be applied in any modes and the result can be analyzed based on it. This transformation can also be applied to the three phase time waves and their phasors, in any case, this transformation will make the input of the three phase independent. The result is that the Clarke transformation only performs the transition from the fuzzy domain to the Modal and does not do anything per se, but for the considered purpose, other relations should be used to achieve the objectives of the problem. For example, in this paper for short circuit calculations and identifying fault phases and locating the fault, some indicators should be defined based on the voltage and current relations in the modal domain and utilize them to this ends (El Sayed Tag El Din et al., 2005).

Indicators of Fault Detection/ Localization

The purpose of online detection and locating of the fault for each line of three-phase is based on the phasor measurement techniques. The general diagram of the comparative detecting/locating technique based on the Fourier transform is shown in Fig.1 on the basis of the equations described in this section.

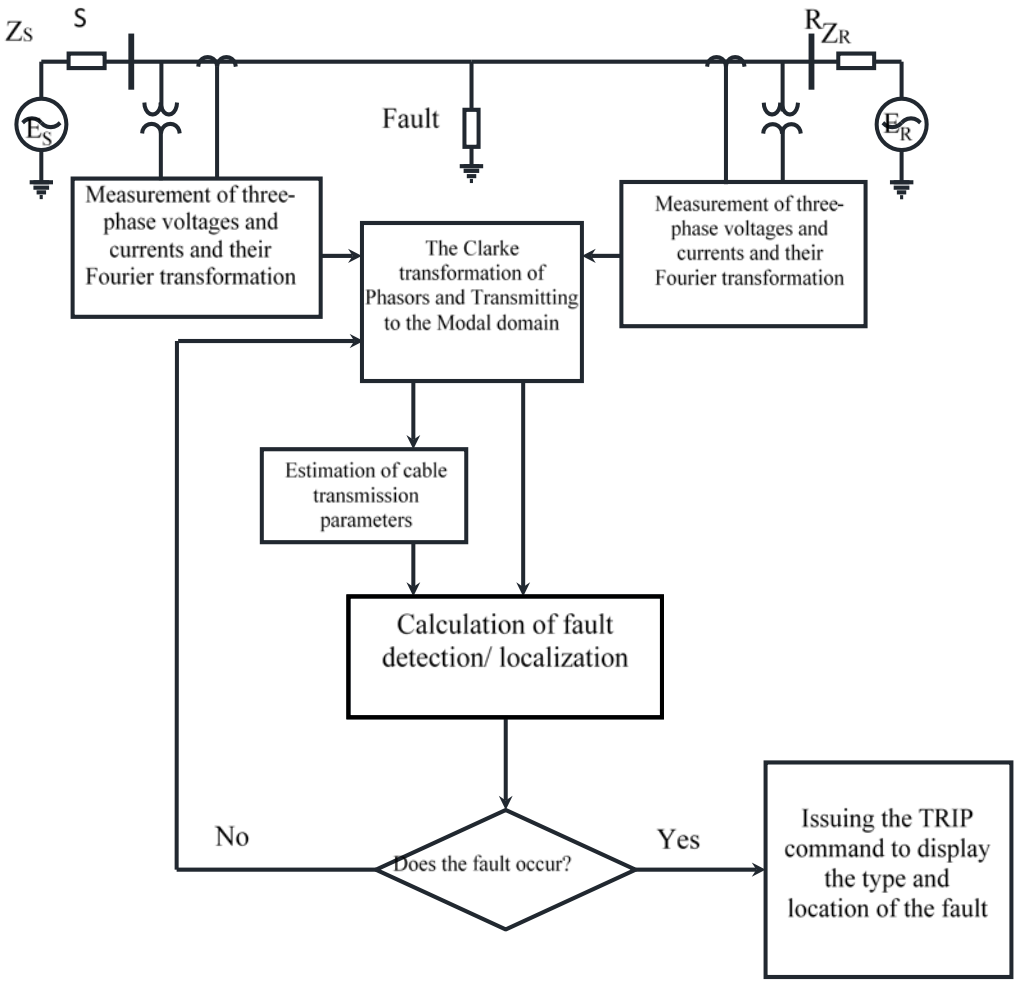

Figure 1: The structure of the comparative detecting/locating of EHV/UHV transmission line based on the Fourier and Modal Transformations and the defining indices.

Voltage and current measurement units are installed at both ends of the line. The three-phase voltages and currents measured at both ends of the line are converted by Fourier transform into phasoric components, the phasors in the fuzzy domain are transmitted by the Clarke transformation into the modal domain, and on the basis of which the transmission line parameters are estimated approximately. Then, using the fault detection and location indicators that are related to the characteristics of the line, the occurrence, the type of fault, and its location will be estimated.

The Simulation and Modeling of Cable Transmission Lines in the EMTP/ATP Software

In this paper, JMarti model is used for underground cables. The single-line diagram of the studied model is presented in Fig. (2). The adjacent cable network model is modeled on both sides of the S and R bus with a voltage source of °10 ∠230 and 230∠0kV. The characteristics of the external networks and their modeling are not considered, because the method of using the detection and location indicators is completely independent of the type of network and depends on the phasor voltage and the current at the two terminal ends connected to the cable.

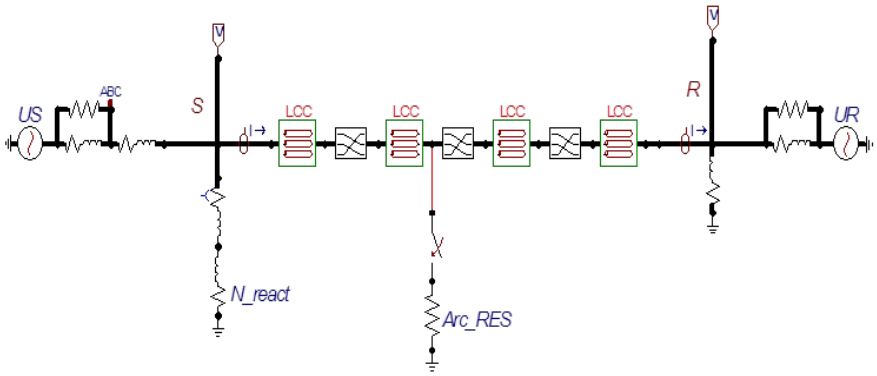

Figure 2. The single-line diagram and infinite bus

In the studied model, the length of cable between the two networks is 40 kilometers and its rated voltage is 230kV. The physical characteristics of the cable are also shown in Table (1).

Table 1. The physical characteristics of XLPE cable with rated voltage of 230kV

The parameter name	Value
Inner radius of core (cm)	0.0
Outer radius of core(cm)	2.34
Inner radius of pit (cm)	3.85
Outer radius of pit (cm)	4.13
External radius of insulation (cm)	4.84
Core resistance (Ω-m)	0.0170×10^{-8}
Insulation resistance (Ω-m)	0.2100×10^{-6}
ε_r for inner insulation	3.5
ε_r for outer insulation	8.0
Relative permeability coefficient μ_r	1.0
Ground resistance (Ω-m)	100

Simulation of Several Types of Faults in Locations and with Different Resistance at Different Times

Having modeled the line and network, the two single-phase faults of AG and BG and two two-phase to ground fault of ABG occur at different points of the line and in 0.3 and 0.305 seconds. First, the fault waveforms will be displayed in the ATP software and then these waveforms will be transmitted to MATLAB software and will be presented along with its phasor representation over time. In addition, waveforms of detection and fault locating indicators are presented in different fault states. Fault resistivity is assumed to be 1, 100 and 100 ohm for fault generating and fault modeling with low arch resistance to high fault resistance. In the representation of the transient waveforms and the discrete Fourier transform performance and the detection and location indicators, the shapes associated with fault created in phase A and the ABG fault are displayed and due to the similarities of other faults, the presentation of related forms is rejected and the results are presented in the relevant tables.

- *Single-phase Fault of A in the Middle of the Cable in 0.3 Seconds with 1 ohm Fault Resistance*

In this section, a single-phase short circuit fault of AG with 1 ohm fault resistance is created at 0.3 seconds in the middle of the cable. It is assumed that the measuring units are installed on

both S and R buses and the voltage and current signals of both ends are measured at any moment. The measured values of voltage and current from both the S and R buses are shown in the following figures, respectively. The voltage waveform in the bus is shown in Fig. (3). As seen in the figure, the voltage is in its steady state before the fault occurs, with a short circuit fault at 0.3 seconds, the voltage drops sharply and after eliminating the fault at 0.5 seconds, it goes back to its normal state.

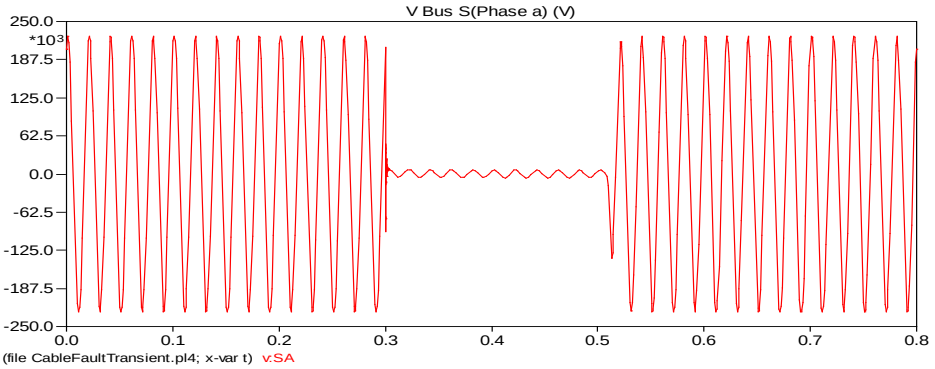

Figure 3. The measured voltage waveform of phase A at the bus S (Horizontal axis of time axis: S and the vertical axis of voltage axis: V)

Having transferred to the MATLAB environment and applying the discrete Fourier transform, the waveform (3) will be redisplayed in Fig. (4). In the present study, waveform time steps in the ATP software range from 6 to 10, and for phasor measurement, the time waveform resulted from ATP with 10 kHz frequency is modeled and it is taken from the samples resulted from discrete Fourier transform with 50 Hz frequency. The sampling window is considered to be a full power cycle and the number of the samples in this window is N=200. Due to the constant number of the samples in the discrete Fourier transform sampling window, there will be a 20 millisecond delay (a power cycle) after the sudden change of waveform state, where the full cycle of discrete Fourier transform will not be able to detect these changes rapidly.

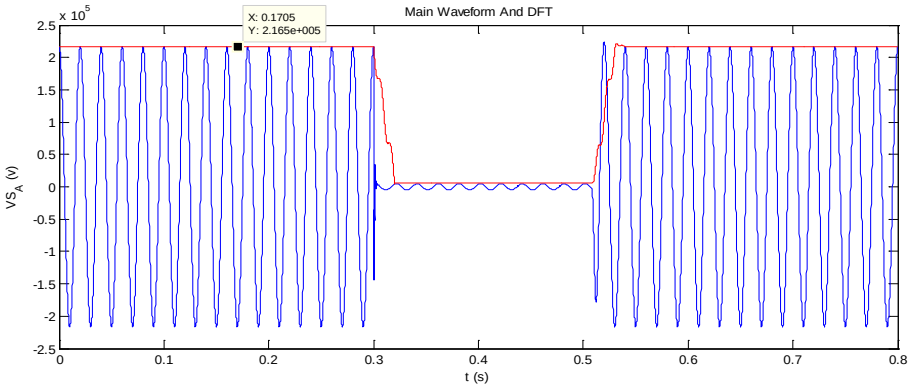

Figure 4. The representation of A waveform in MATLAB environment and the discrete Fourier transform diagram

In order to prevent the phase rotation from moving the information window of the discrete Fourier transform along the waveform, a recurring discrete Fourier transform is used, so that

the sinusoidal waveform angle remains constant during steady state. The result of this operation is shown in Fig. (5). Figure (6) shows the voltage angle measured at the bus S.

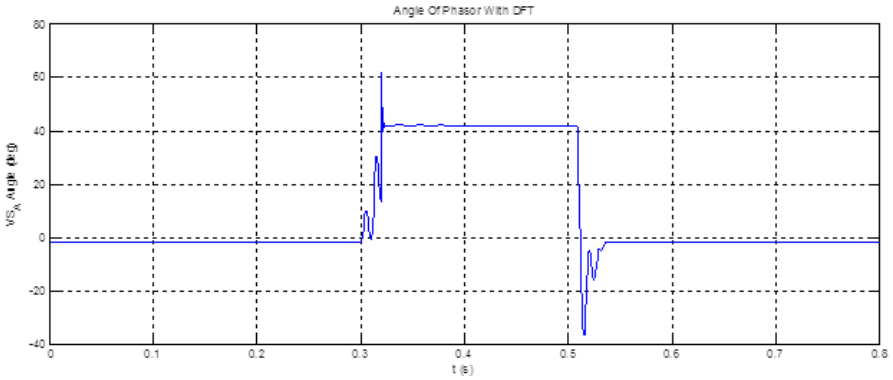

Figure 5. Phase voltage angles of A at bus S

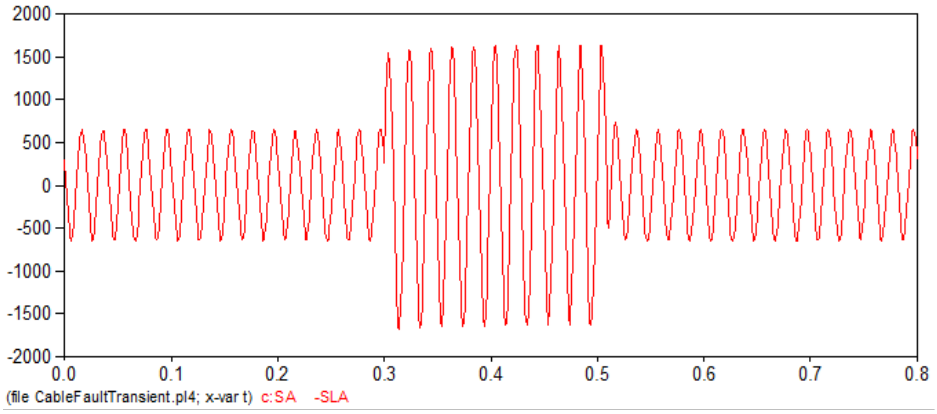

Figure 6. The waveform of the measured phase of A at bus S (Horizontal axis of time axis: S and vertical axis of current axis: A)

Due to the short circuit occurrence in the current waveform, a DC reduction component may occur with different amplitudes. In Fig. 6, the DC component is presented in a small waveform. The sampled waveform of the phase A stream at the S-bus and its size in the MATLAB environment is plotted in Fig. 7. Figure 8 shows the phase angle A of the S-bus.

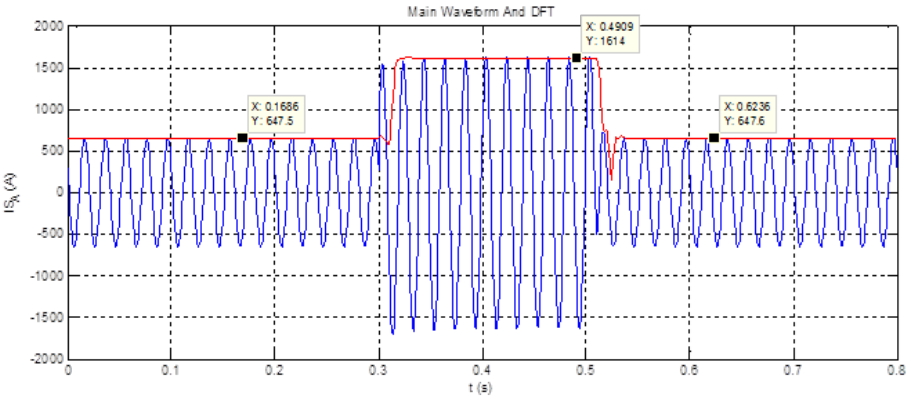

Figure 7. The waveform of sampled current at bus S

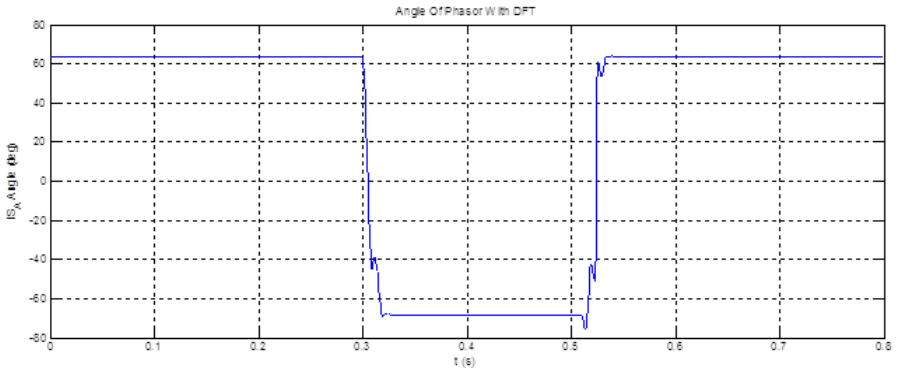

Figure 8. The angle of phase current A at bus A

The waveform of voltage of the phases of B and C during the phase fault A is stable and uniform which is presented in Fig (9) and (10) regarding the time waveform of voltages of two phase at EMTP/ATP and the size of voltage of phase B.

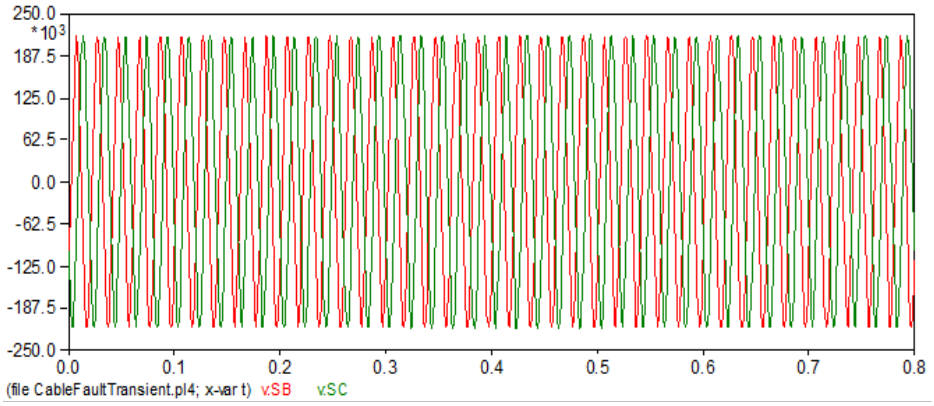

Figure 9. Voltages of Phase B and C at bus S (Horizontal axis of time axis: S and vertical axis of voltage axis: V)

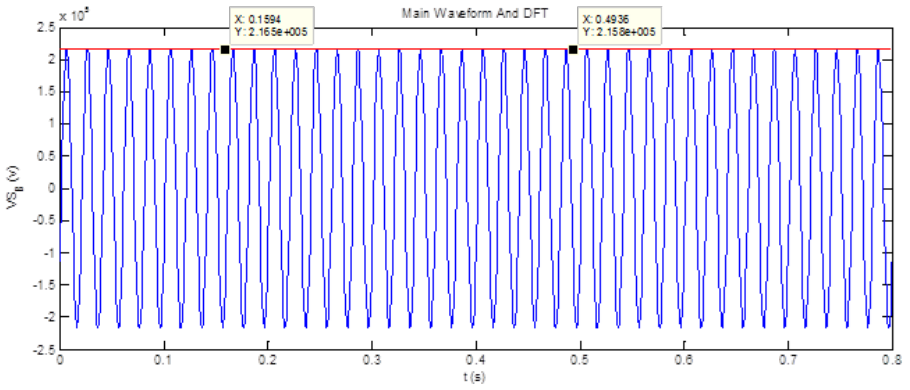

Figure 10. The size of voltage of phase B at bus S

Figure (11) shows the voltage angle of phase B when the fault occurs at phase A, according to the Figure it can easily be observed that this change is at a range of 0.25 degree and is negligible. This change shows the coupling rate and the effect of the variation of a phase in

two other phases and expresses the dependence between them. According to the simulation forms, this dependence can be easily detected. The waveform (12) also shows the waveforms of the current phase of B and C. With a little more detailed observation in the time waveform, the change in current phases of B and C can be detected at the initial time and solving the fault. The current phase B and its size are shown in Fig (13). Changes in the true waveform and its size in this figure are more evident. Similarly, the phase angle of the B current phase is shown in Fig (14). The variations in the angle of the current are about 0.3 degrees and have a small amount.

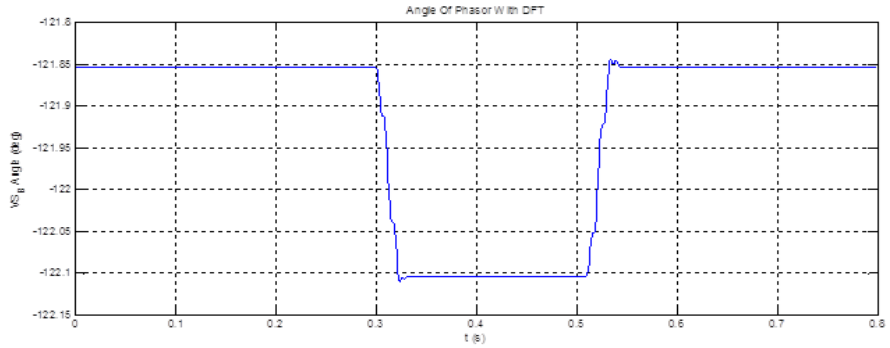

Figure 11. Phasor angle of voltage phase B at bus S

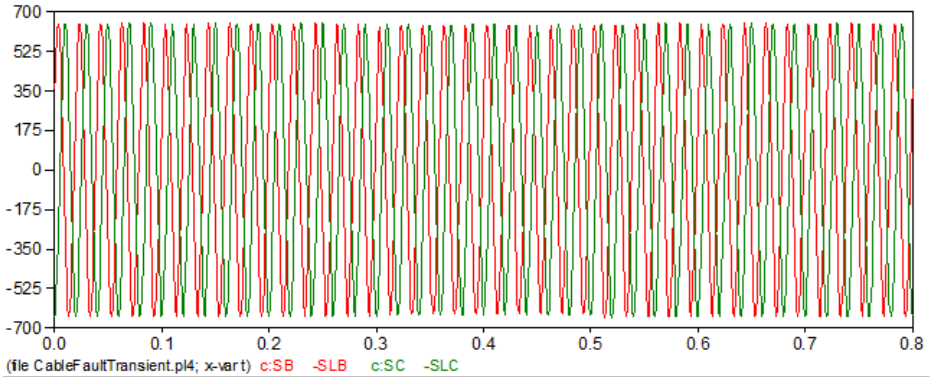

Figure 12. The current of phases B and C at bus S (Horizontal axis of time axis: S and vertical axis of current axis: A)

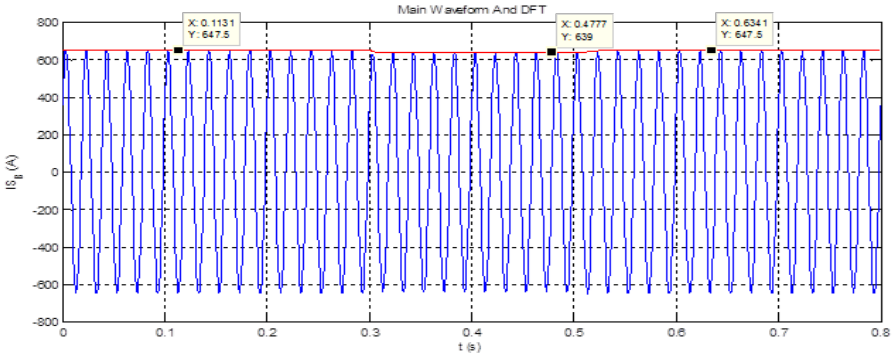

Figure 13. The waveform of current phase B

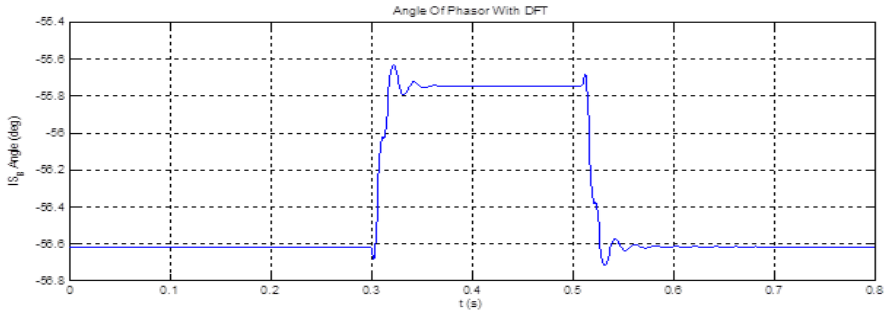

Figure 14. Phasor angle of current phase B

Figure (15) shows the fault detection indicator $N_{a, b, c.}$ It can be observed from the figure that all the three parameters of fault detection in the moments before the fault is equal to zero, but after a fault occurred in phase A, the value of $N_a$suddenly increases from zero to a large amount at 0.3 seconds, if the values of N_b and N_c are still equal to zero and do not change, they will be continuously equal to zero. After eliminating the fault, the value of the fault detection indicator of phase A (N_a) decreases again to zero. Simultaneously, Figure (16) shows the value of the fault detection indicator in three modes of α, β and 0, as shown, all three fault indicators of N_α ,N_β and N_0 before the fault are equal to zero, and as soon as the fault occurs the magnitude will increase and after eliminating the fault in phase A, they return to zero. By observing this state of affairs, it can be easily understood that, although the Modal detection indicators are suitable for detecting the fault situation, the type of fault cannot be correctly identified with these indices.

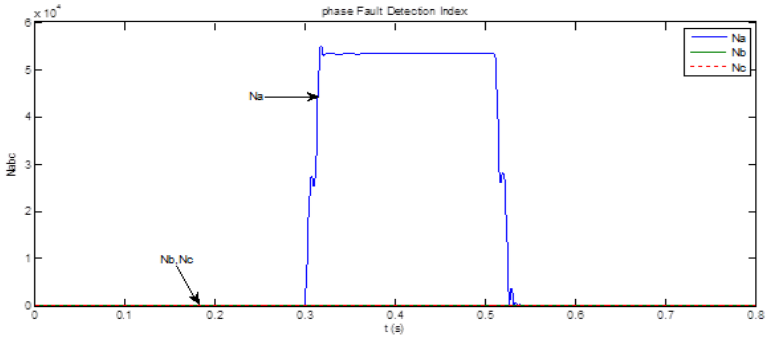

Figure 15. The detection indicator of phase fault

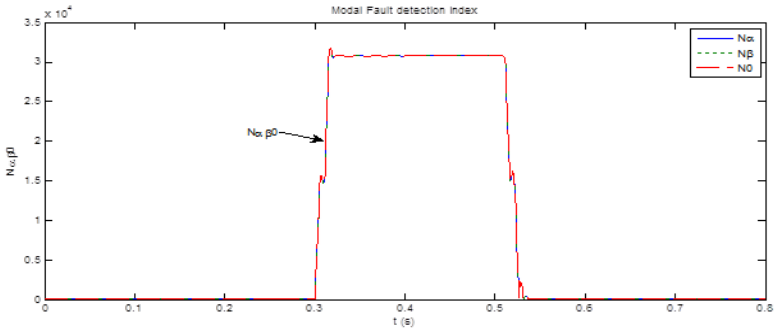

Figure 16. The detection indicator of Modal fault $N_{\alpha\beta0}$

Figure (17) shows the values of fault locating indices in the Modal domain for the three modes α ،β and zero $D_{\alpha\beta 0}$. It is noticeable that the values of this index in three modes before the error have different values greater than one. Once the error occurs in phase A, in 0.3 seconds, all three indexes of D_α ،D_β and D_0 are 0.5.

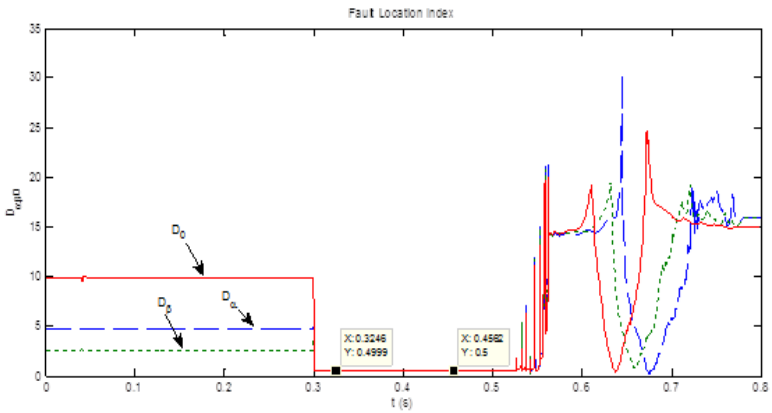

Figure 17. The locating indicators of fault $D_{\alpha,\beta,0}$

- *The Single-phase Fault A in the Middle of Cable with 100 ohm and 1000 ohm Resistances*

With the creation of 100 ohm fault at 0.3 seconds, the voltage value is much lower than the previous one and increase of the current is also lower than the previous one. This also holds true for the voltage and current angle. Figure (18) shows the size and angle of the phase A voltage at the S-bus. Although the angle of the current changes greatly during the fault. Figure (19) also shows the same diagrams for the bus current S. The waveforms of the N, M, and D detection and location indicators are shown in the following figures, respectively.

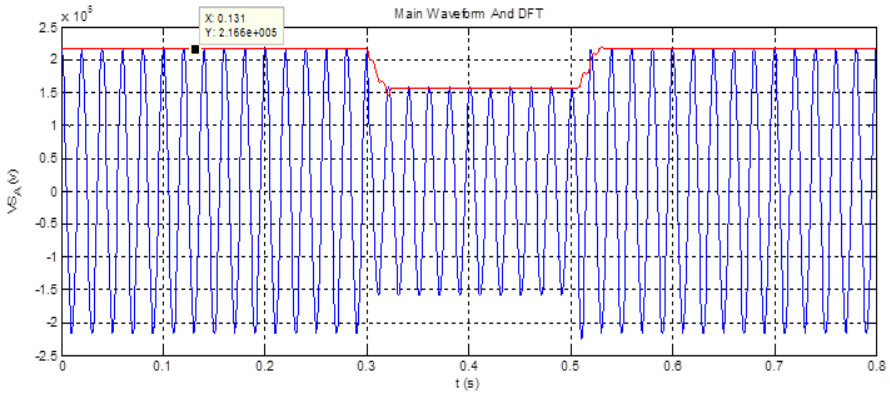

A) The waveform of voltage phase A

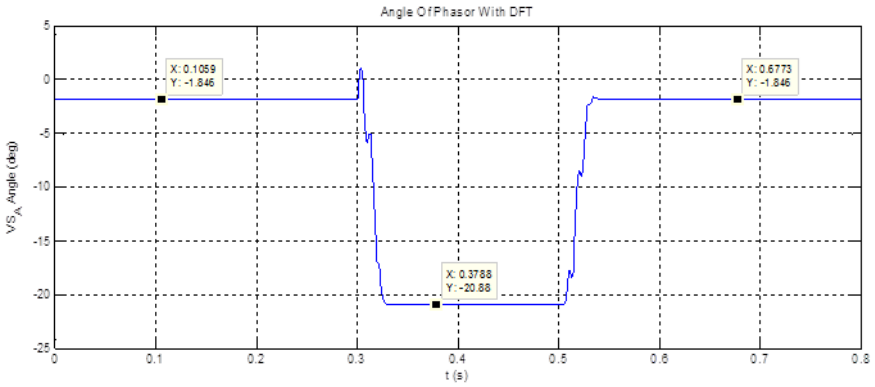

B) The angle of voltage phase A

Figure 18. The size and angle of voltage phase A

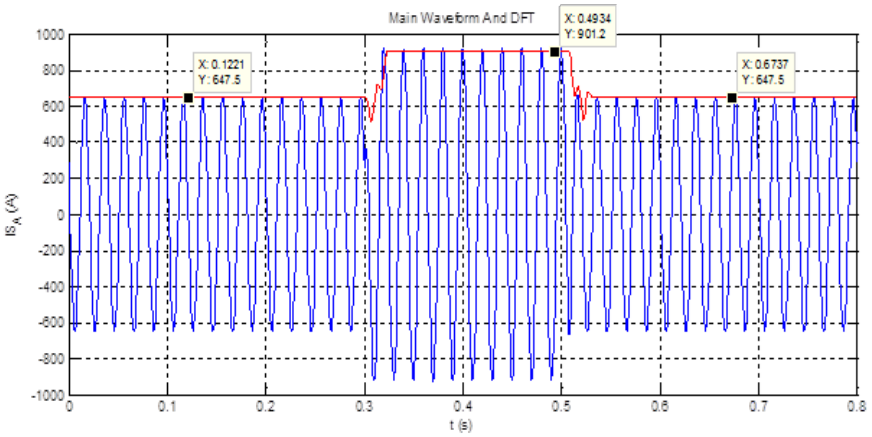

A) The waveform of current phase A

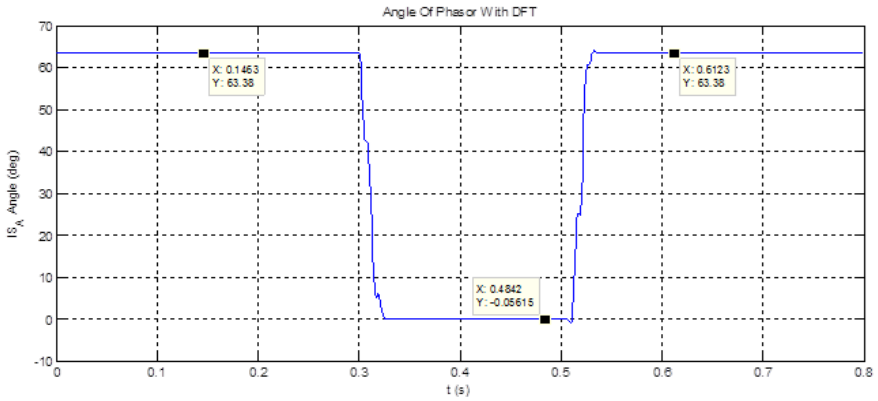

B) The angle of current phase A

Figure 19. The size and angle of current phase A at bus S

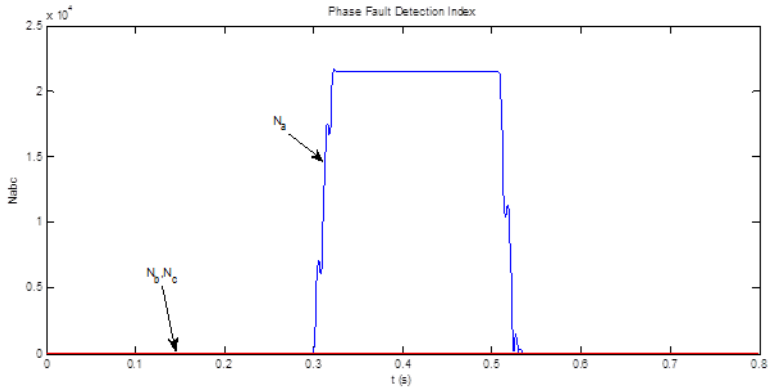

Figure 20. The detection indicator of fuzzy fault

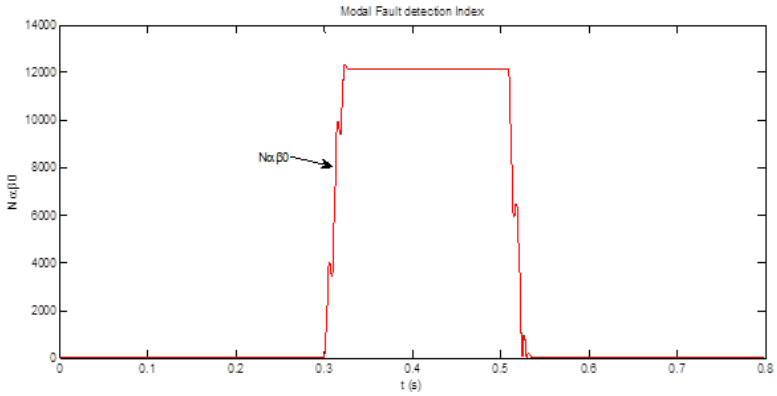

Figure 21. The detection indicator of Modal fault $N_{\alpha\beta0}$

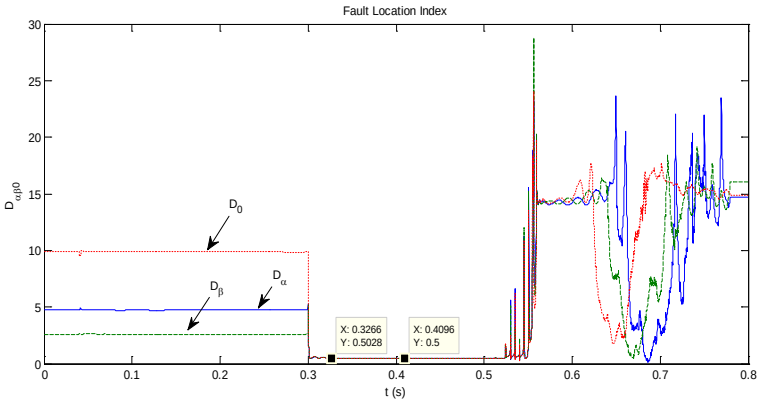

Figure 22. The locating indicators of fault $D_{\alpha,\beta,0}$

It should be noted that despite the significant increase in error resistance, the values of detection and error detection parameters in this case, without any problems, have yielded quite accurate results and the results are similar to the first one. Even fault phase detection of healthy phases in high power failure conditions is difficult due to the close proximity of voltage and current. Again, the above-mentioned forms for a 1000 ohm resistance error state, but this time it is displayed at the R-bus. The waveform of the voltage and current in the bass R is shown in Figures 23 and 24, respectively.

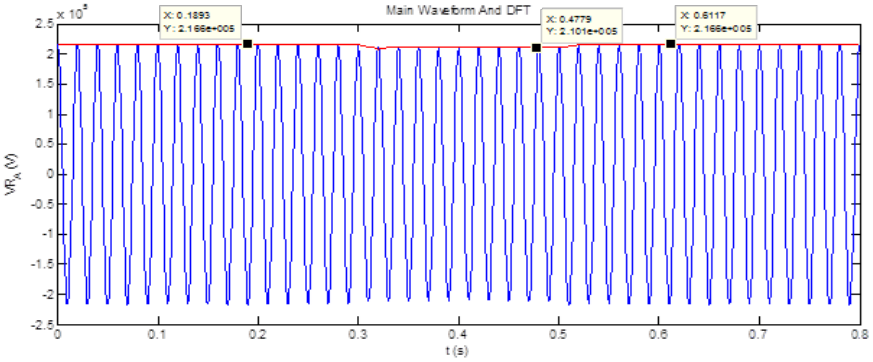

A) The waveform voltage phase A

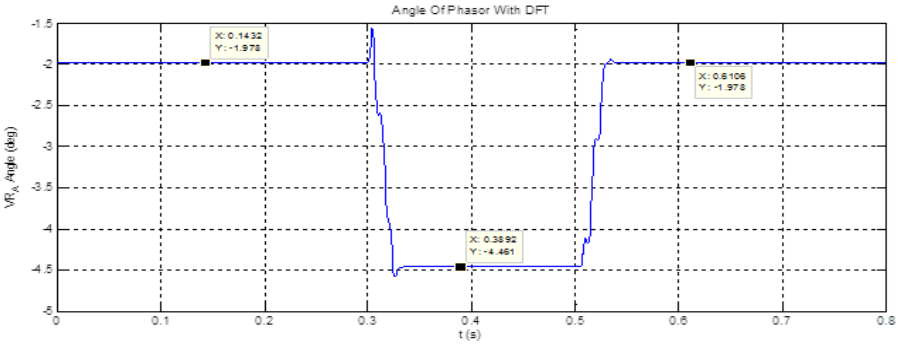

B) The voltage phase angle A

Figure 23. The size and angle of phase voltage A at bus R

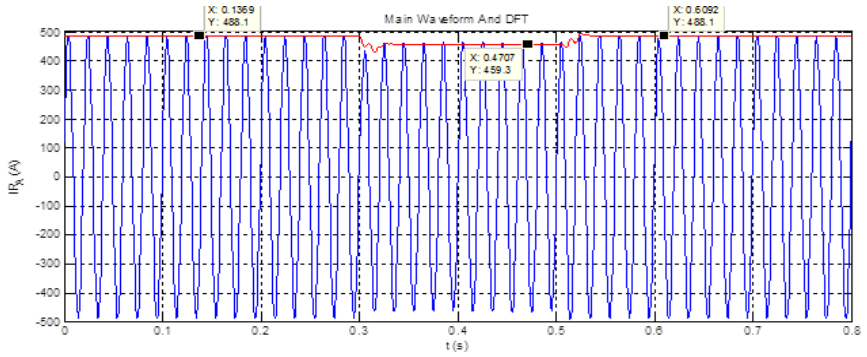

A) The waveform of current phase A

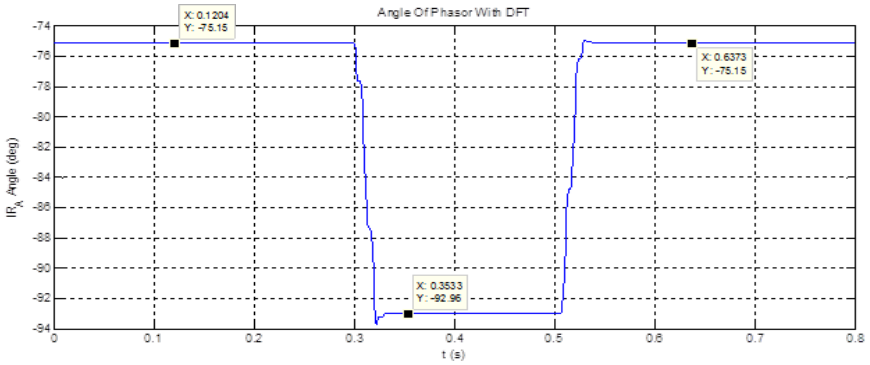

B) The angle of current phase A

Figure 24. The size and angle of current phase A at bus R

The waveform of the current in the bus S is also shown in Fig. (25). As you can see, the variations of the voltage and the current waveforms are very small. As a result of visual observation, the occurrence of the fault is not probable and if only the size of the waveform is considered for comparison, a true judgment cannot occur between the fault condition and other conditions such as instantaneous overload and other conditions. Even the most interesting issue in the waveforms of the two sides is that although the bus current S is slightly increased, even with the source at bus side R, the value of measurement in bus R at the fault moment, it is even less than its normal value. If the impedance method is used for this kind of error, the probability of error in it will be high, but there will be no problem using the indicators of detection and location because of the use of information from both sides. The error indicators are given in the following figures.

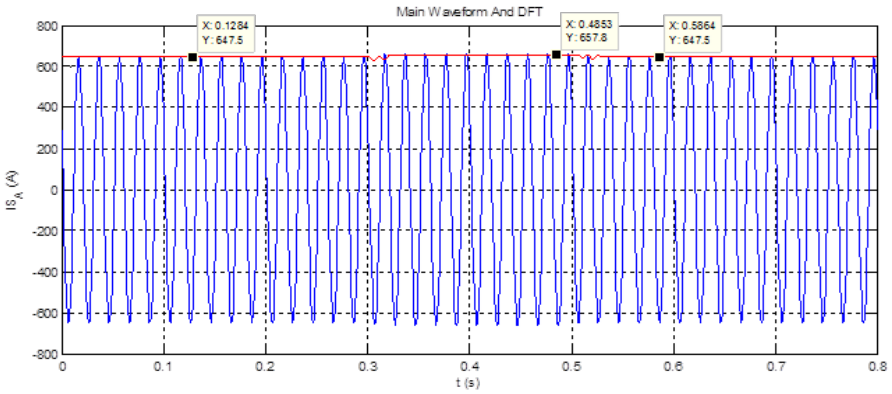

A) Current waveform of phase A

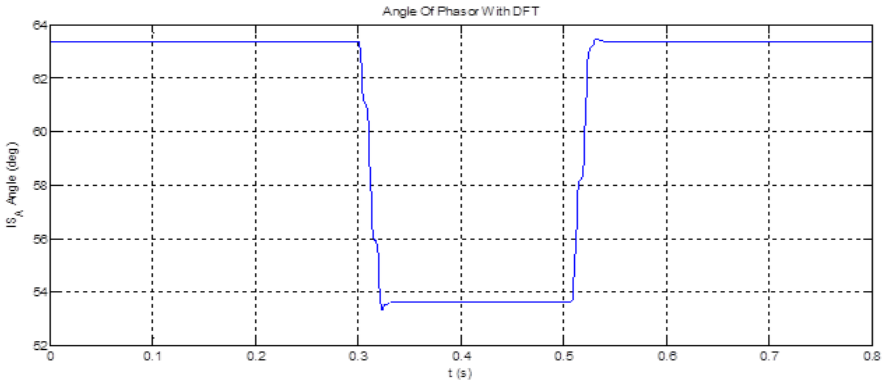

B) Current angle of phase A

Figure 25. The size and angle of current phase A in the bus S

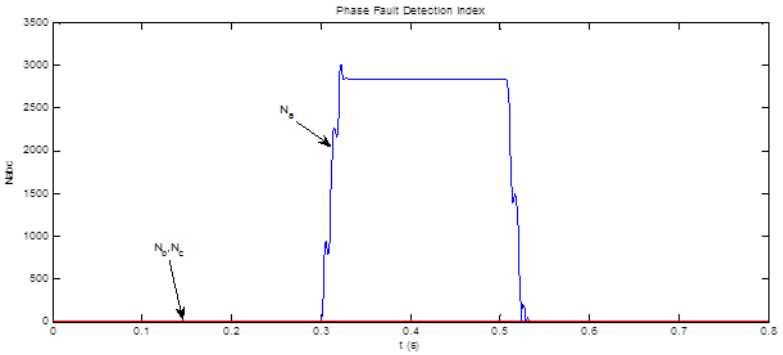

Figure 26. The detection indicator of fuzzy fault

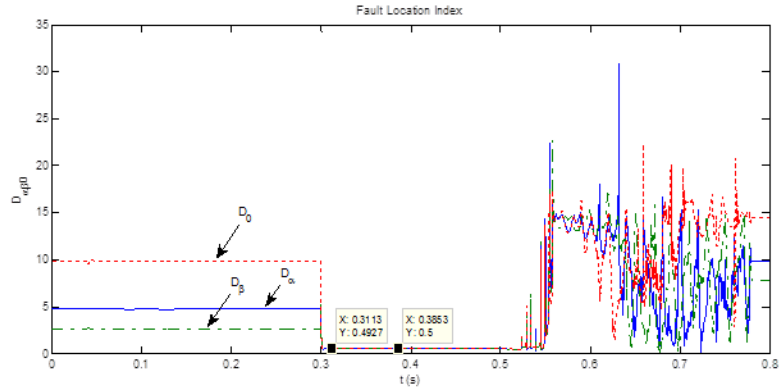

Figure 27. The locating indicators of fault $D_{\alpha,\beta,0}$

- *1 ohm Single-phase Fault at 0.3 Seconds in Phase B in the Middle of the Cable*

The response to the single-phase fault is displayed in phase B. The values of detection and fault locating indicators are presented in Figures (28) and (29).

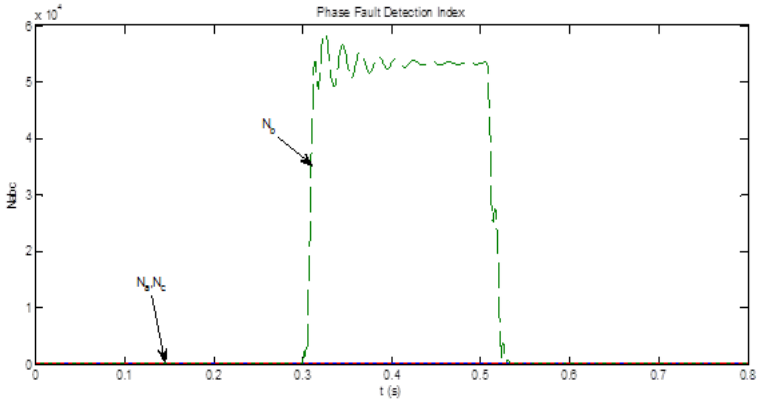

Figure 28. The detection indicator of fuzzy fault

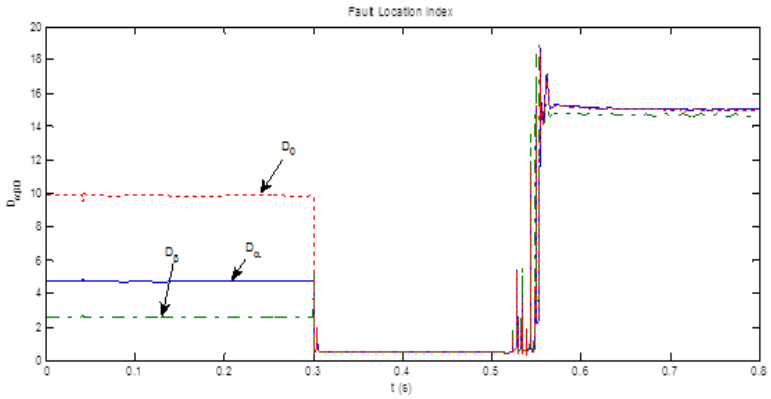

Figure 29. The locating indicators of fault $D_{\alpha,\beta,0}$

Comparison of the Results of Various Types of Faults

In this section, the relevant simulation of AG and BG single-phase faults and ABG two-phase fault for 1, 100 and 1000 ohm fault at 0.3 seconds and 0.305 seconds in different points of the cable at 50% and 25% cable length resistance at bus R is given in the respective tables and the type and locations of the calculated fault and the time and calculation faults are presented. The calculations of other faults in different places and times can also be done and the results can be observed.

Table 2. Types of fault created in the middle of the cable and the indicators of detection and location and their diagnosis time

Time of finding the fault location with the percentage of the fault	The percent of locating fault indicator	The fault localization (kilometer)	The amount of locating fault indicator	Time of detecting the type of fault (seconds)	The performance of detection indicators of fuzzy fault	Time of fault occurrence (seconds)	Fault resistance (ohm)	Type of fault	The distance of fault from the source S
0.3262	0.0123	20.0025	0.4999	0.3006	Na, Ma(100%)	0.3	1	AG	20km
0.4289	0.1611	20.0322	0.4991	0.307	Na, Ma(100%)	0.305			
0.3327	0.0234	20.0047	0.4998	0.3017	Na, Ma(100%)	0.3	100		
0.3382	0.0043	20.0009	0.4999	0.3083	Na, Ma(100%)	0.305			
0.3415	0.0016	20.0003	0.4999	0.3115	Na, Ma(100%)	0.3	1000		
0.3425	0.012	20.0024	0.4999	0.3187	Na, Ma(100%)	0.305			
0.3956	-0.1688	19.9662	0.5008	0.3013	Nb, Mb(100%)	0.3	1	BG	
0.3656	0.1847	20.0669	0.4991	0.3057	Nb, Mb(100%)	0.305			
0.3349	0.0053	20.0011	0.4999	0.3055	Nb, Mb(100%)	0.3	100		
0.3399	0.024	20.0048	0.4999	0.3068	Nb, Mb(100%)	0.305			
0.3395	0.0361	20.0072	0.4999	0.3159	Nb, Mb(100%)	0.3	1000		
0.3439	-0.0021	19.9996	0.5000	0.3169	Nb, Mb(100%)	0.305			
0.3676	0.1661	20.0332	0.4992	0.3014	Na, Ma, Nb, Mb(100%)	0.3	1	ABG	
0.4176	-0.1555	19.9689	0.5008	0.3064	Na, Ma, Nb, Mb(100%)	0.305			
0.3316	0.0092	20.0018	0.5000	0.3024	Na, Ma, Nb, Mb(100%)	0.3	100		
0.3359	-0.0195	19.9968	0.5001	0.3017	Na, Ma, Nb, Mb(100%)	0.305			
0.3409	0.0065	20.0013	0.5000	0.3063	Na, Ma, Nb, Mb(100%)	0.3	1000		
0.3419	0.0253	20.0051	0.4999	0.3094	Na, Ma, Nb, Mb(100%)	0.305			

In Table (2), the minimum error is related to a short-circuit AG with a resistance of 1000 ohms at 0.3 seconds, which is 0.0016%, which is 41.5 millisecond after an error occurring, equivalent to two power cycles. Of course, the delay of a cycle is related to the completion of the Fourier transformation information window completion process. Apart from AG and ABG errors, an ohmic time of 0.305 seconds in other cases, with increasing error resistance, is observed relatively, the error location time has increased in addition to the detection time. In the case of error accuracy, the result is approximately the opposite, that is, with an increase in error resistance, the accuracy of the error also increased relatively. As can be said, with more time spent locating, the error is reduced, and this is normal. With the observation and comparison of all the states specified in the table and their results, it is easy to determine the efficiency of using the combined method of this dissertation. According to the above table, in the worst case, the distance between the computed error location is 36.9 meters in 40 kilometers and at best 30 cm in relation to the correct location.

Table 3. Errors generated in 25% of cable relative to bus R and detection and location indicators and their detection time

Time of finding the fault location with the percentage of the fault	The percent of locating fault indicator	The fault localization (kilometer)	The amount of locating fault indicator	Time of detecting the type of fault (seconds)	The performance of detection indicators of fuzzy fault	Time of fault occurrence (seconds)	Fault resistance (ohm)	Type of fault	The distance of fault from the source S
0.3388	0.1042	30.0313	0.2492	0.3090	Na, Ma(100%)	0.3	1	AG	30km
0.4689	-0.1022	29.9693	0.2508	0.3069	Na, Ma(100%)	0.305			
0.3326	0.0117	30.0035	0.2499	0.3016	Na, Ma(100%)	0.3	100		
0.3391	-0.0090	29.9973	0.2501	0.3082	Na, Ma(100%)	0.305			
0.3407	0.0039	30.0012	0.2500	0.3114	Na, Ma(100%)	0.3	1000		
0.3429	0.0253	30.0076	0.2498	0.3193	Na, Ma(100%)	0.305			
0.4655	-0.0790	29.9763	0.2506	0.3018	Nb, Mb(100%)	0.3	1	BG	
0.4255	-0.1214	29.9636	0.2509	0.3059	Nb, Mb(100%)	0.305			
0.3355	0.0107	30.0032	0.2499	0.3054	Nb, Mb(100%)	0.3	100		
0.3395	0.0241	30.0072	0.2498	0.3067	Nb, Mb(100%)	0.305			
0.3389	0.0403	30.0121	0.2497	0.3158	Nb, Mb(100%)	0.3	1000		
0.3436	0.0085	30.0025	0.2499	0.3168	Nb, Mb(100%)	0.305			
0.4275	-0.1152	29.9654	0.2509	0.3012	Na, Ma, Nb, Mb(100%)	0.3	1	ABG	
0.4575	0.1231	30.0369	0.2491	0.3067	Na, Ma, Nb, Mb(100%)	0.305			
0.3368	-0.1238	29.9988	0.2500	0.3023	Na, Ma, Nb, Mb(100%)	0.3	100		
0.3366	-0.0118	29.9965	0.2501	0.3071	Na, Ma, Nb, Mb(100%)	0.305			
0.3401	0.0104	30.0031	0.2499	0.3064	Na, Ma, Nb, Mb(100%)	0.3	1000		
0.3452	0.0048	30.0015	0.2500	0.3095	Na, Ma, Nb, Mb(100%)	0.305			

In Table (3), the minimum fault of 0.9 ms, and the highest of 18.8 ms, is related to the 1000-ohm single-phase fault at 0.305 seconds. The lowest fault in the calculation of the locating indicator is 0.009%, which is equivalent to a 2.7 cm longitudinalfaultrelative to 40 km. On the other hand, the highest fault in the ABG two-phase fault with a 1-ohm resistor appears at 0.305 seconds, and the fault of this indicator is 0.1231%, which is 36.9 meters. In the case of

location time, the minimum time is related to the fault of the AG of 100 ohms at 0.3 seconds with a location fault of 0.0117%, which is 32.6 milliseconds, and the maximum time, as in the previous state, for an AG fault of 0.305 seconds equal to 163.9 milliseconds S is seen.
The absolute calculated values must also be calculated on the basis of the length of the short line, which the reference articles (El Sayed Tag El Din et al., 2005; KANG Ming-cai et al., 2012; Qi-neng Jiang et al., 2010) does not specify the total length of the power cable, although the magnitude of the fault of location is based on the percentage of comparison and is important. It is clear from Table (4) that the short-circuit location fault in this thesis is far less than references (El Sayed Tag El Din et al., 2005; KANG Ming-cai et al., 2012; Qi-neng Jiang et al., 2010) and expresses the superiority of the method proposed in this paper to other methods such as wavelet transform. Meanwhile, the time and type of fault, and the total length of the cable, are not included in this reference.

Table 4. Evaluation of the proposed method than other methods

Method	The percent of fault	The fault location
Wavelet transform	4.48	512
Fit curve	3.36	508
The proposed method of the article	3.26	506

RESULTS

In this paper, the use of Fourier transform as a powerful tool in obtaining the size and angle of each phase is proposed, which obtains complete information on voltage parameters and power grid flows. An online approach is proposed using Fourier transform data on both sides of a cable line that uses detection and location indicators in both the modal and fuzzy domains, and its excellent utilization is shown. The use of Clarke transformation and transition to the modal domain for the independence of the components used to study a variety of studies including fault has been proposed which in addition to reducing the volume of equations caused by the dependence between fuzzy components, it also increase the degree of assurance of the accuracy of the results. The delay of faultdetection and location indicators is very negligible and limited to the delay caused by the Fourier transform calculations. In addition, the accuracy of the calculations of these indicators is very high, and in this case, most of the fault is due to the essence of the Fourier transformation. The responsesof fault detectionindicators in the modal and even fuzzy domains are also correct in 100% of cases. The maximum computational fault caused by the fault locationindicator in the modal domain was less than 5.0%. The precision of the proposed hybrid approach is more than just a number of methods, such as wavelet transform.

References

Aziz M. M. A., El Din E. S. T., Ibrahim D. K.L, and Gilany M., "A phasor-based double ended fault location scheme for aged power cables," Electric Power Components and Systems, vol. 34, pp. 417–432, 2006.

Bewley L. V., "Traveling waves on transmission systems," Trans. of the American Institute of Electrical Engineers, vol. 50, no. 2, pp. 532-550, 1931.227

El Sayed Tag El Din, Mahmoud Gilany, Mohamed Mamdouh Abdel Aziz, "An PMU Double Ended Fault Location Scheme for Aged Power Cables", Power Engineering Society General Meeting, 2005. IEEE, Vol. 1, pp.80 – 86, June 2005.

El Sayed Tag El Din, Mahmoud Gilany, Mohamed Mamdouh Abdel Aziz, "A Wavelet-Based Fault Location technique for Aged Power Cables", Power Engineering Society General Meeting, 2005. IEEE, Vol. 3, pp.2485 – 2491, June 2005.

Gale P. F., Crossley P. A., Xu B., Ge Y., Cory B. J., and Barker J. R. G., "Fault location based on travelling waves," in Proc. Fifth International Conference on Developments in Power System Protection, pp. 54-59, Mar. 30-Apr. 1, 1993.

Hassan Sayed Barakat Shimaa, "Fault detection, classification and location in Underground Cables", A Thesis Submitted to Faculty of Engineering - Fayoum University in Partial Fulfillment of the Requirements for Degree of Master of Science, 2014.

KANG Ming-cai, WEI Yang, ZHANG Jun-fang, HU guang, Yingning Qiu, "Power cable fault location based on mathematical morphology and wavelet theory", Sustainable Power Generation and Supply (SUPERGEN 2012), International Conference on, pp. 1 – 6, Sep 2012.

Kuan K. K. and Warwick K., "Real-time expert system for fault location on high voltage underground distribution cables," IEE Proceedings C: Generation, Transmission and Distribution, vol. 139, no. 3, pp. 235-240, May 1992.

Phadke A.G., Thorp J.S., "Synchronized Phasor Measurements and Their Applications", Virginia Polytechnic Institute and State University Blacksburg, VA USA, Springer Science and Business Media, LLC 2008, ISBN 978-0-387-76535-8.

Provoost F. and Van Buijtenen W., "Practical experience with fault location in MV cable networks," in Proc. 20th International Conference on Electricity Distribution, Paper no. 0527, June 8-11, 2009.

Qi-neng Jiang, Shu-tao Zhao, Jun Zhao and Chen-guang Zhao, "A Power Cable Fault Location Method Combining with Wavelet Analysis and Curve Fitting", Electricity Distribution (CICED), 2010 China International Conference on, pp. 1 – 5, Sep 2010.

"Underground cable fault location reference manual," Electric Power Research Institute, TR-105502, Nov. 1995.

Van Oirsouw P. M. and Provoost F., "Fault localization in an MV distribution network," in Proc. 17th International Conference on Electricity Distribution, pp. 2-6, May 12-15, 2003.

Yang X., Choi M. S., Lee S. J., Ten C. W., and Lim S. I., "Fault location for underground power cable using distributed parameter approach," IEEE Trans.Power System, vol. 23, no. 4, pp. 1809-1816, Nov. 2008.